

**NASA Contractor Report 178053**

**ICASE REPORT NO. 86-5**

NASA-CR-178053  
19860011253

# ICASE

APPLICATION OF A RUNGE-KUTTA SCHEME  
FOR HIGH-SPEED INVISCID INTERNAL FLOWS

Anutosh Moitra

Eli Turkel

Ajay Kumar

Contract Nos. NAS1-17070 and NAS1-18107

January 1986

LIBRARY COPY

MAR 14 1986

LANGLEY RESEARCH CENTER  
LIBRARY, NASA  
HAMPTON, VIRGINIA

INSTITUTE FOR COMPUTER APPLICATIONS IN SCIENCE AND ENGINEERING  
NASA Langley Research Center, Hampton, Virginia 23665

Operated by the Universities Space Research Association



National Aeronautics and  
Space Administration

**Langley Research Center**  
Hampton, Virginia 23665



**APPLICATION OF A RUNGE-KUTTA SCHEME  
FOR HIGH-SPEED INVISCID INTERNAL FLOWS**

Anutosh Moitra

SASC Technologies, Inc., Hampton, Virginia 23665

Eli Turkel

Institute for Computer Applications in Science and Engineering

NASA Langley Research Center, Hampton, Virginia 23665-5225

and

Tel-Aviv University

Ajay Kumar

NASA Langley Research Center, Hampton, Virginia 23665-5225

**ABSTRACT**

A multi-stage Runge-Kutta method is analyzed for solving the two-dimensional Euler equations for external and internal flow problems. Subsonic, supersonic and, highly supersonic flows are studied. Various techniques for accelerating the convergence to a steady state are described and analyzed. Effects of the grid aspect ratio on the rate of convergence are evaluated. An enthalpy damping technique applicable to supersonic flows is described in detail. Numerical results for supersonic flows containing both oblique and normal shocks are presented confirming the efficiency of the method.

---

Research was supported by the National Aeronautics and Space Administration under NASA Contract Nos. NAS1-17070 and NAS1-18107 while the second author was in residence at ICASE, NASA Langley Research Center, Hampton, VA 23665-5225.



## I. INTRODUCTION

Over the past few years, a number of numerical schemes have been devised for solving the compressible Euler equations. An explicit finite-volume scheme with multi-stage Runge-Kutta integration in time, as proposed by Jameson, Schmidt, and Turkel [1], has shown promise of being an efficient and accurate Euler solver. This method has been found to be of great versatility in the simulation of transonic flow, particularly when the method has been augmented by such convergence accelerating techniques as local time-stepping, enthalpy damping, and implicit residual averaging. The incorporation of these techniques as described by Turkel [2] has produced remarkable increases in the rate of convergence to a steady-state. However, the extent to which these enhancements are necessary vary significantly from one problem to another. Although the preceding method has been used successfully for transonic flow, its use in high-speed flows involving shocks of substantial strength has not been explored fully. Moitra [3] has presented some results for supersonic flow demonstrating the possibility of its use in capturing complex shock structures. The aim of this study is to investigate the applicability, accuracy, and efficacy of the multi-stage Runge-Kutta method in solving the compressible Euler equations for two-dimensional supersonic internal flow problems involving complex shock discontinuities of substantial strength. The qualitative and quantitative nature of the effects of various techniques for accelerating the convergence to a steady-state are analyzed in detail. The results from the present calculations are compared with experimental data and results obtained by other numerical methods [4,5].

## II. SOLUTION ALGORITHM

The Runge-Kutta time-stepping scheme is more efficient than many other explicit schemes such as MacCormack's original scheme. In addition, the steady-state solutions are independent of the time-step, and as mentioned earlier, the scheme is amenable to a variety of techniques for accelerating steady-state convergence. Before the results are presented, we present a description of these accelerating techniques.

### Local Time-Stepping

A variable time-step determined by the bound on the local Courant number is used in each zone. The use of the largest time-step at any location allowed by the local stability bound accelerates convergence to the steady-state at the expense of time-accuracy of the solution.

### Implicit Residual Averaging

This strategy for accelerating convergence consists of taking an average of residuals in neighboring cells by the following expression

$$\epsilon R_{i-1} + (1-2\epsilon)R_i + \epsilon R_{i+1} = \bar{R}_i \quad (1)$$

where  $R_i$  denotes the residual in the  $i$ -th cell and  $\bar{R}_i$  is the residual before the implicit averaging. This is done after every even stage of the scheme. This results in a scheme which is stable for a CFL number  $\lambda$  if

$$\epsilon > \frac{1}{4} \left\{ \left( \frac{\lambda}{\lambda^*} \right)^2 \right\} - 1 \quad (2)$$

where  $\lambda^*$  is the CFL limit of the original scheme. Since  $\lambda$  can be much higher than  $\lambda^*$ , the rate of convergence is accelerated. However, choosing too large a CFL limit,  $\lambda$ , slows down the convergence. An optimal choice is  $\lambda/\lambda^* \sim 2$ . See reference [2] for further details.

### Artificial Dissipation

The method requires artificial dissipative terms in order to alleviate two difficulties associated with centrally differenced schemes. The first one is that of odd-even point decoupling that adversely affects convergence. Addition of a fourth-difference artificial viscosity reduces this difficulty. The second difficulty manifests itself in oscillations in the vicinity of shocks. An additional viscous term is introduced, which is an approximation to a second derivative in order to overcome this problem. To maintain second-order accuracy this term contains a coefficient that itself depends on the second difference of the pressure. Since the fourth-order difference can create oscillations near the shock, it is turned off in the vicinity of shocks.

### Enthalpy Damping

The enthalpy damping procedure has been modified from the original version [1] of FL052 in order to enable it to be used in supersonic flow. Hence, we shall describe the new enthalpy damping in more detail.

In solving the full potential equation it is well known that adding artificial terms such as  $\phi_t$  can accelerate the convergence to a steady state. For a first-order system of equations such as the Euler equations, this can not be done. Instead, it is suggested [1] that one can add forcing

functions that depend on  $h-h_0$ ,  $h = (E+P)/\rho$ ; where  $h$  and  $h_0$  denote the local and the free stream values of the total specific enthalpy. In the steady state, the total specific enthalpy  $h$  is constant along each streamline in an inviscid flow. Assuming that the flow comes from a common reservoir, in the steady state  $h = h_0$  everywhere, where  $h_0$  is determined by the inflow boundary conditions. Based on the analogy with the full potential equations and the fact that  $h - h_0 \propto \phi_t$ , it was suggested that the forcing function be added to the density equation. Using density  $\rho$  and velocity components  $(u,v)$  the modified equations are

$$\rho_t + L_1 = -\alpha\rho(h - h_0) \quad (2a)$$

$$u_t + L_2 = 0 \quad (2b)$$

$$v_t + L_3 = 0, \quad (2c)$$

where  $L_j$  are the usual space derivatives of the Euler equations. When one solves for the momentum variables  $\rho u$  and  $\rho v$ , then the forcing function also occurs in these equations so that

$$(\rho u)_t + L_{2m} = -\alpha\rho u(h - h_0) \quad (3a)$$

$$(\rho v)_t + L_{3m} = -\alpha\rho v(h - h_0) \quad (3b)$$

where the subscript  $m$  denotes the space derivative terms in the momentum equations. The finite difference approximation to the density equation is

$$\rho^{n+1} - \rho^n = -\Delta t L_1 - \alpha \Delta t \rho^{n+1} (h^n - h_0) \quad (4)$$

or

$$\rho^{n+1} = \frac{\rho^n - \Delta t L_1}{1 + \alpha \Delta t (h^n - h_0)} \quad (5)$$

Freezing coefficients and changing variables [2], one can reduce (2) to a second-order equation for  $\rho$ ,

$$\rho_{\tau\tau} - (c^2 - u^2)\rho_{\eta\eta} + 2K\rho_{\tau} = 0 \quad (6)$$

where  $\eta$  and  $\tau$  are new independent variables and the positive constant  $K$  depends on  $1 - M^2$  and linearly on  $\alpha$ . Thus, we obtain the potential-like equation with the artificial term  $K\rho_{\tau}$ . To see the effect of  $K$ , we assume that  $\rho$  has the simple form

$$\rho = e^{\beta\tau} e^{i\xi\eta}, \quad -\pi < \eta < \pi. \quad (7)$$

Assuming subsonic flow, letting  $q^2 = c^2 - u^2$  and substituting (7) into (6), we find

$$\beta^2 + 2K\beta + q^2 \xi^2 = 0$$

or

$$\beta = -K + \sqrt{K^2 - q^2 \xi^2} \quad (8)$$

In order to reach a steady state as fast as possible we wish the real part of  $\beta$ , i.e.,  $\text{Re } \beta$  to be as negative as possible. Note for  $K = 0$ , i.e., no

enthalpy damping,  $\text{Re } \beta = 0$  and we have no term driving the system to a steady state. We see from (8) that  $\text{Re } \beta$  is most negative when  $0 < K < q\xi$ , and  $K$  is as large as possible. Thus, we wish to choose  $K$  slightly less than  $q\xi$ .

We first consider the case in which we want to damp the low frequencies, since these are the slowest to decay. In this case, we have  $\xi = O(1)$  and so  $K = O(1)$ . We stress that the constant HM in the FLO52 code is equal to  $\alpha\Delta t$ . Hence, if  $\alpha = O(1)$ , this implies that HM should vary linearly with  $\Delta t$  and therefore, is very small. We next consider the case where we wish to damp the high frequencies, e.g., multigrid applications. Now  $\xi \approx \pi/\Delta\eta$  and so  $K$  varies as  $1/\Delta\eta$  or equivalently  $1/\Delta t$ . In this case,  $\text{HM} = \alpha\Delta t$  should be a constant.

This analysis implies that the enthalpy damping suggested in [1] is useful if:

- (1) the flow is locally subsonic;
- (2a) HM is proportional to  $\Delta t$  to damp low frequencies;
- (2b) HM is constant to damp high frequencies.

In order to explain the effectiveness of the enthalpy damping for non-multigrid applications and to extend its usefulness to supersonic applications we must discuss the energy equation which was ignored in (2). Since the enthalpy damping was originally based on an analogy with the full potential equation there is no obvious way to treat the energy equation. The original idea was to append to (2) the equation

$$\frac{\partial s}{\partial t} + L_{4s} = 0, \quad (9)$$

i.e., nothing special is done to the entropy equation. Rewriting (9) for the energy equation we obtain

$$\frac{\partial E}{\partial t} + L_{4E} = -\alpha(h - h_0)h.$$

However, now the forcing function contains a quadratic term in  $h$  and was found to be destabilizing rather than stabilizing. To avoid this difficulty an ad hoc correction was used and the energy equation became

$$\frac{\partial E}{\partial t} + L_{4E} = -\alpha(h - h_0). \quad (2d)$$

Instead of the ad hoc procedure, we shall replace (9) by

$$\frac{\partial h}{\partial t} + L_{4h} = -\beta(h - h_0). \quad (9')$$

Thus, instead of ignoring the entropy we try and drive the total enthalpy to its steady state value. We note that if  $\beta = \infty$  we recover the isoenergetic approximation in which the energy equation is replaced by Bernoulli's law. Thus, our new system is a compromise between the original Euler equations and the isoenergetic equations. Of course, in the steady state all of these variations are equivalent. Eliminating  $h$  we can rewrite (9') as

$$\frac{\partial E}{\partial t} + L_{4E} = -\left(\alpha E + \frac{\beta \rho}{\gamma}\right)(h - h_0). \quad (2d')$$

We thus, conclude that enthalpy damping helps in the non-multigrid version of FL052 because of the energy equation and not because of the continuity

equation, i.e., we can set  $\alpha = 0$  in (2) and the coefficient  $\beta$  assumes the important role. This improved enthalpy damping can be used equally well in supersonic regions. Furthermore, one can choose  $\beta$  as large as one desires without causing instabilities, while choosing too large an  $\alpha\Delta t$  causes instabilities. However, choosing  $\beta$  too large may slow down the convergence rate. In all the cases presented in the results section we chose  $\alpha = 0$  and  $\beta\Delta t$  to be constant.

Combining all the previous discussions we prescribe for the system (2a), (3a), (3b), and (2d') that:

(1) For locally supersonic flow we must have  $\alpha = 0$ . For locally subsonic flow we advise choosing  $\alpha$  to depend on  $1 - M^2$ . The coefficient  $\beta$  in (2d') can be used for both subsonic and supersonic flows and does not depend on the Mach number.

(2) To dampen the low frequencies,  $HM = \alpha\Delta t$  should depend linearly on  $\Delta t$  while to damp the high frequencies,  $HM = \alpha\Delta t$  should be chosen to be constant. The choice of  $\beta$  is frequency independent, but  $\beta\Delta t$  should be constant. Hence, even for a multigrid version one should choose  $\alpha\Delta t$  and  $\beta\Delta t$  independently, especially since  $\alpha$  should depend on  $1 - M^2$ .

### III. RESULTS

A wide variety of test cases involving different Mach numbers and shock strengths were investigated in order to assess the ability of the numerical scheme to simulate flows ranging from subsonic to high supersonic Mach numbers. Convergence histories for the different test cases are presented with a view to establishing the nature and extent of the effects of the

different convergence accelerating techniques as well as different grid sizes. The CPU-seconds execution times presented are those for scalar processing on a CDC Cyber-175 processor. Computed results have been compared with experimental data and results from other schemes whenever available.

### Test Case 1

The first case investigated is the inviscid shock reflection problem in which an incident shock wave of prescribed strength reflects off a flat plate. A schematic of the configuration is presented in Figure 1. Uniform grids with various numbers of points in the x-direction ( $0 < x < 4.0$ ) and the y-direction ( $0 < y < 1.5$ ) were considered. At the inflow boundary for  $y > 1$  and along the upper boundary all dependent variables are specified based on a prescribed incident shock-angle  $\alpha$ . All variables are extrapolated from the interior at the supersonic outflow boundary.

The first set of computations for this configuration was performed with a grid of 51 points in the x-direction and 31 points in the y-direction. The shock-incidence angle  $\alpha$  was  $29^\circ$ . A contour plot of the computed pressures appears in Figure 2. Both the incident and the reflected shocks are seen to be reasonably sharp. In Figure 3, a comparison of the pressure profile at the  $y = 0.25$  line computed by the present method with results obtained by the original MacCormack scheme [4] and the Osher [5] upwind scheme is presented and a good agreement of the results is noticed. Next, a set of convergence histories corresponding to the use of the different convergence accelerating techniques, is presented in Figure 4. The use of a locally maximum time step is seen to substantially increase the rate of convergence over that obtained by using a global minimum time step. The use of enthalpy damping does not

create any advantage for this particular configuration; however, the beneficial aspects of enthalpy damping will be apparent in the results presented for the next test case. Finally, the use of the implicit residual averaging technique results in a slight further increase in the convergence rate. In all these plots the logarithm of the residual, i.e., the average value of the time derivative of density, is plotted against actual CPU seconds of computation.

The next series of computations for this configuration were done in order to ascertain the effect of the grid aspect ratios on the rate of convergence. Seven uniform grids of different sizes were used to compute the flow with  $M_\infty = 2.9$  and  $\alpha = 29^\circ$  and the corresponding normack scheme [4] and the Osher [5] upwind scheme is presented and a good agreement of the results is noticed. Next, a set of convergence histories corresponding to the use of the different convergence accelerating techniques, is presented in Figure 4. The use of a locally maximum time step is seen to substantially increase the rate of convergence over that obtained by using a global minimum time step. The use of enthalpy damping does not create any advantage for this particular configuration; however, the beneficial aspects of enthalpy damping will be apparent in the results presented for the next test case. Finally, the use of the implicit residual averaging technique results in a slight further increase in the convergence rate. In all these plots the logarithm of the residual, i.e., the average value of the time derivative of density, is plotted against actual CPU seconds of computation.

The next series of computations for this configuration were done in order to ascertain the effect of the grid aspect ratios on the rate of convergence. Seven uniform grids of different sizes were used to compute the flow with

$M_\infty = 2.9$  and  $\alpha = 29^\circ$  and the corresponding convergence histories are presented in Figure 5. The different aspect ratios of the cells are seen to have pronounced effects on the convergence rates. The fastest rates of convergence were generated by three particular grids, namely those with  $41 \times 25$ ,  $51 \times 31$ , and  $61 \times 37$  points. These three grids have a cell aspect ratio of approximately 1.62. A departure from this value of the cell aspect ratio is seen to substantially slow the rate of convergence. This indicates that the convergence of the finite-volume Euler scheme is strongly influenced by the aspect ratio of the computational cells. We next consider the possibility that the angle of the shock may have some influence on the value of the cell aspect ratio for which the fastest rate of convergence is attained. To test this hypothesis an additional series of computations were performed for the same configuration with the shock angle  $\alpha$  changed to  $23^\circ$ , all other parameters remaining the same. The resulting convergence histories are plotted in Figure 6. As is immediately obvious, the grid sizes with cell aspect ratio of 1.62 again give rise to the fastest convergence rates. A departure from this value, as in the case of the  $51 \times 43$  grid, is again seen to result in substantial worsening of the rate of convergence. This leads to the conclusion that moderate changes in the shock angle do not substantially influence the value of the optimal cell aspect ratio for which the fastest convergence rate is achieved.

## Test Case 2

The next test cases involved internal flow in a single throat nozzle [6]. Flow regimes ranging from subsonic to highly supersonic in nature have been investigated. A variety of complex shock-structures have been successfully

captured. At supersonic inflow boundaries all variables are specified and at supersonic outflow all the variables are extrapolated from the interior. For subsonic inflow boundaries characteristic-type boundary conditions are applied. At outflow boundaries characteristic extrapolation is supplemented by a radiation boundary condition. A uniform grid of  $61 \times 31$  points is used in all of these computations.

A fully supersonic internal flow is considered as the first test problem with this configuration. In this problem Mach 3.5 flow enters the two-dimensional nozzle which is symmetric about the centerline. A contour plot of the computed pressures is presented in Figure 7. A complex shock structure consisting of multiple-reflected shocks is noticed. Interaction of the expansion fan emanating from the nozzle wall with the shock reflected off the centerline is clearly visible in the throat region. This demonstrates the ability of the present Euler method to capture repeatedly reflected shock structures at moderately high supersonic Mach numbers. The effects of the various convergence accelerating strategies are apparent in the convergence histories plotted in Figure 8. Enthalpy damping, in this case substantially increases the rate of convergence. The use of implicit residual averaging is seen to remarkably accelerate convergence and causes an approximately 200 seconds reduction in the computational time required to reach the same level of the residual as that in the case of enthalpy damping alone.

The next problem provides a more severe test of the solution procedure's ability to capture shocks and to handle subsonic and supersonic flow regions in the configuration. The incoming flow is subsonic at a Mach number of 0.46. The flow accelerates as it travels down the nozzle and becomes supersonic at the throat creating a supersonic region in the middle section of the

nozzle. This supersonic region ultimately terminates at a normal shock beyond which the flow is again subsonic. The terminal shock is clearly visible in the pressure-contour plot presented in Figure 9. The presence of these different flow regimes do not necessitate any special treatments as far as the algorithm is concerned. A comparative plot of surface pressure computed by the present algorithm and available experimental data [6] is presented in Figure 10. The agreement of the results is noticeably good and confirms the ability of the method to predict complex internal flows accurately. Some experiments at hypersonic Mach numbers have been performed by the authors and the results obtained generated encouragement as to the applicability of the method to computation of hypersonic flow.

#### IV. CONCLUSIONS

Enthalpy damping, heretofore restricted in its applicability to subsonic flows, has been demonstrated to be successfully applicable to supersonic flows. Significant savings in computational time have been achieved by the use of the present enthalpy damping technique. Problems involving supersonic and subsonic flow regions have been solved successfully demonstrating the versatility of the Runge-Kutta scheme. A particular value of the cell aspect ratio is seen to cause the fastest rate of convergence; however, moderate changes of the shock angle are not seen to have significant influence on this value of the aspect ratio.

**REFERENCES**

- [1] Jameson, A.; Schmidt, W.; and Turkel, E.: Numerical solutions of the Euler equations by finite volume methods using Runge-Kutta time-stepping schemes. AIAA Paper No. 81-1259, 1981.
  
- [2] Turkel, E.: Acceleration to a steady state for the Euler equations. Numerical Methods for the Euler Equations of Fluid Dynamics, SIAM, 1985, pp. 281-311.
  
- [3] Moitra, A.: Numerical solution of the Euler equations for high-speed, blended wing-body configurations. AIAA Paper No. 85-0123, 1985.
  
- [4] Kumar, A.: Numerical analysis of the scramjet inlet flow field by using two-dimensional Navier-Stokes equations. NASA TP-1940, 1981.
  
- [5] Chakravarty, S. R. and Osher, S.: High resolution applications of the Osher upwind scheme for the Euler equations. AIAA Paper No. 83-1943, 1983.
  
- [6] Boger, T. J.; Sajben, M.; and Kroutil, J. C.: Characteristic frequency and length scales in transonic diffuser flow oscillations. AIAA Paper 81-1291, 1981.

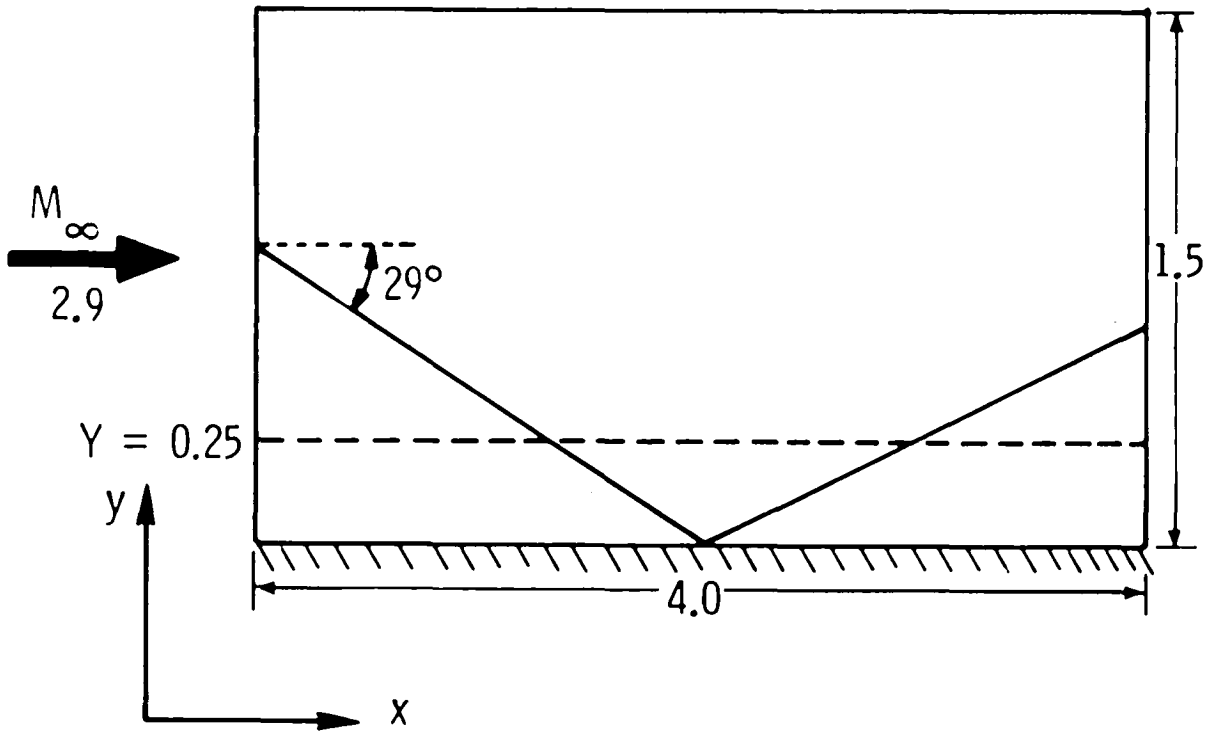


Figure 1. Configuration of 2-D shock-reflection problem.

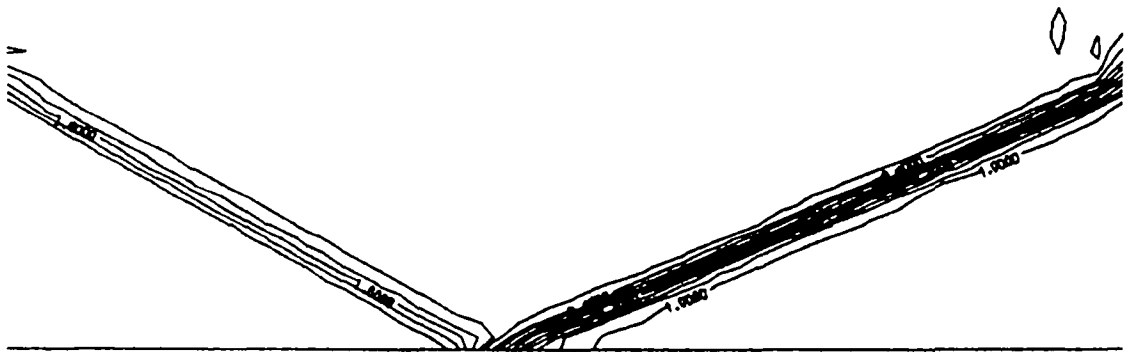


Figure 2. Contour plot of computed pressure for 2-D shock-reflection.

$$M_\infty = 2.9, \alpha = 29^\circ.$$

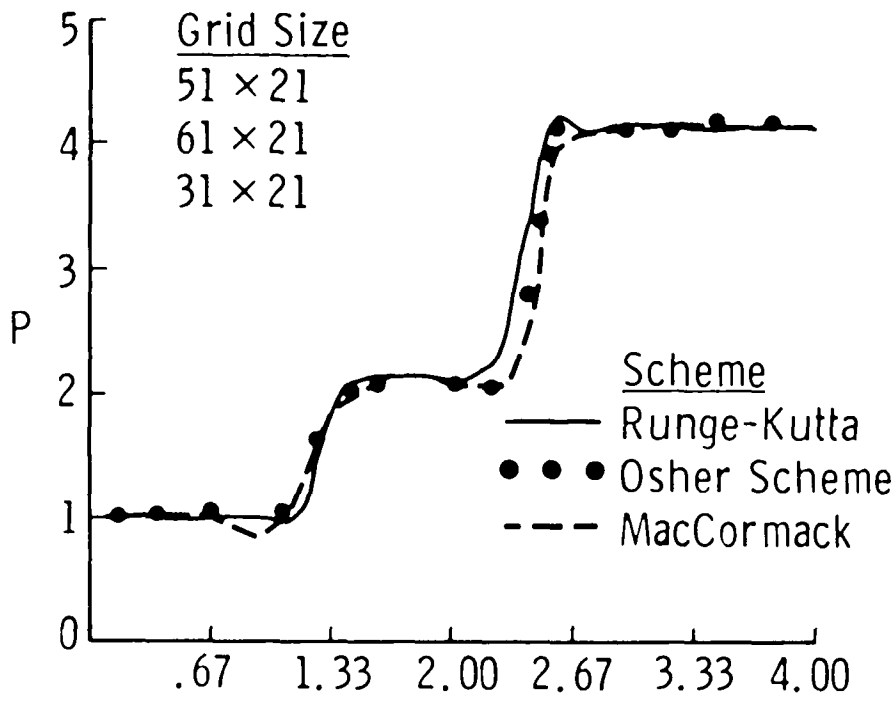


Figure 3. Plot of computed pressure at  $y = 0.25$  for 2-D shock reflection.  $M_\infty = 2.9$ ,  $\alpha = 29^\circ$ .

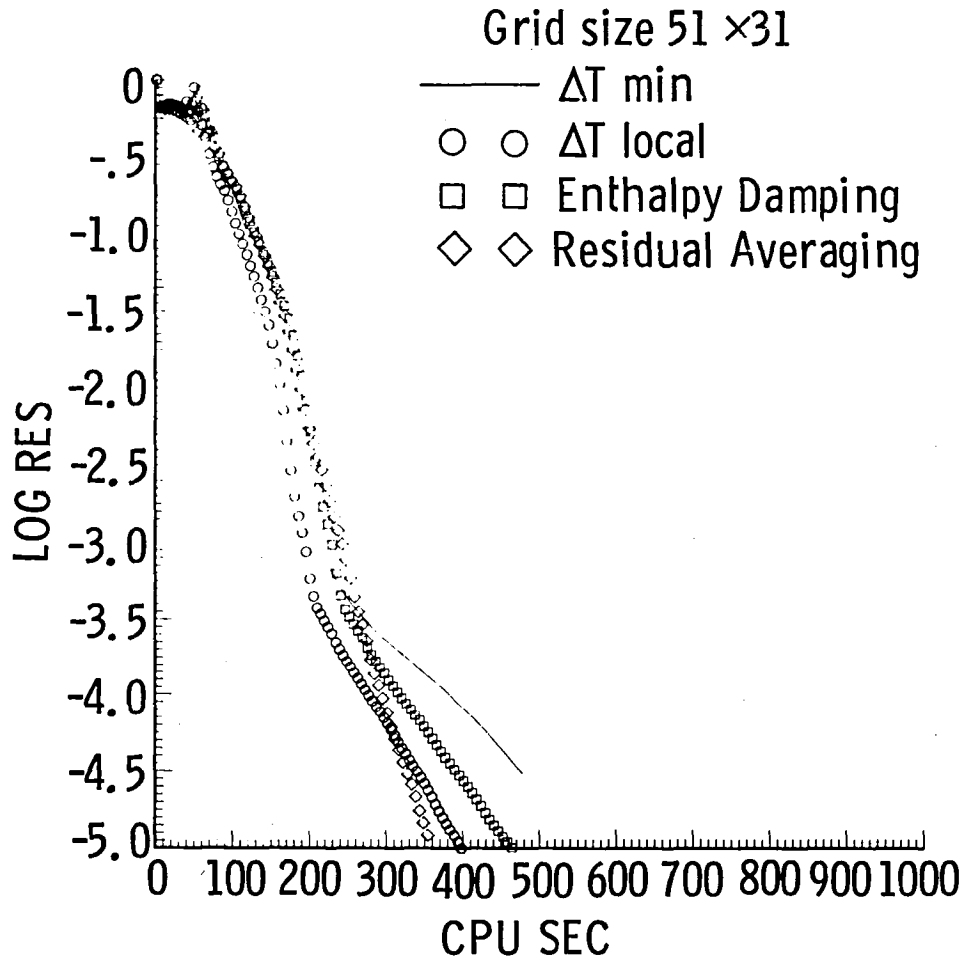


Figure 4. Convergence histories for different accelerating techniques for 2-D shock-reflection.  $M_\infty = 2.9$ ,  $\alpha = 29^\circ$ , Grid: 51 × 31.

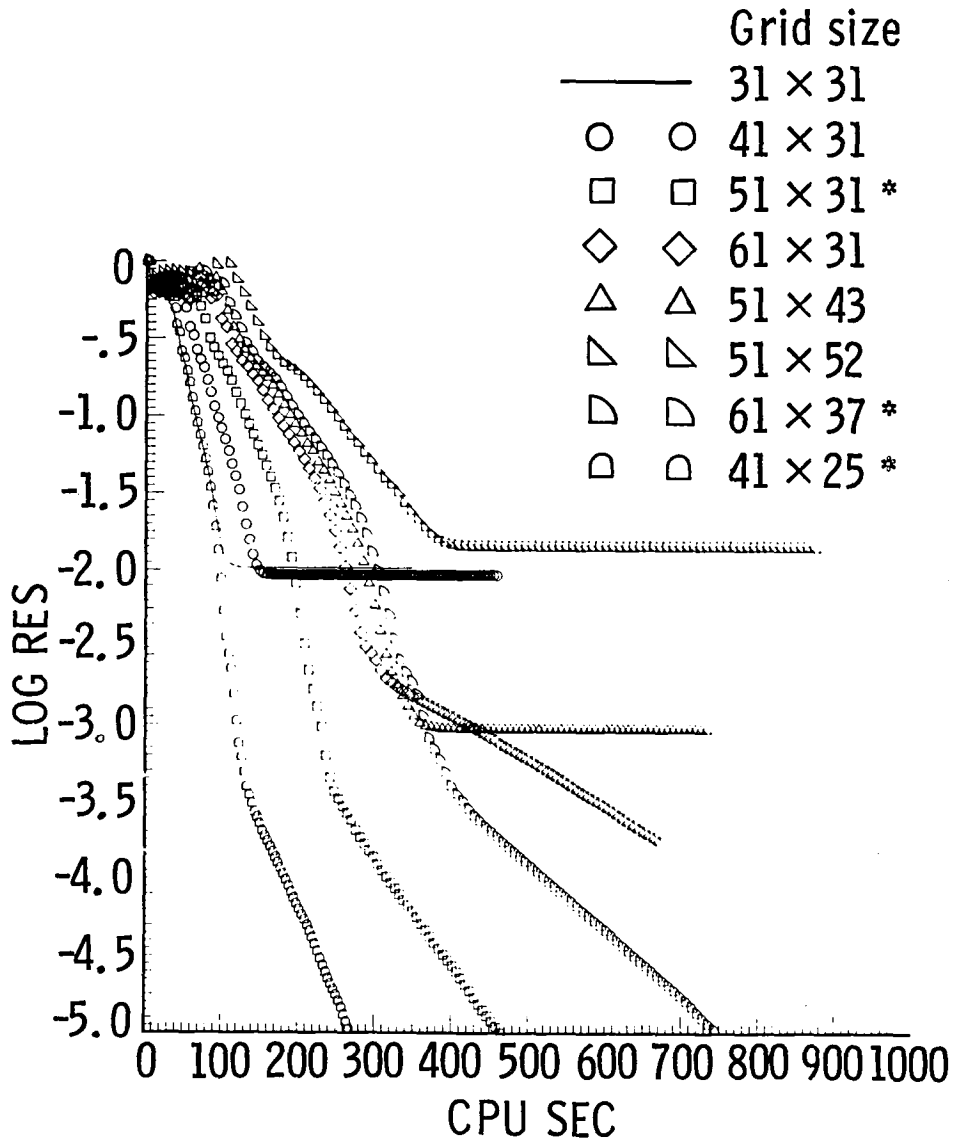


Figure 5. Convergence histories for different grid sizes for 2-D shock reflection.  $M_\infty = 2.9$ ,  $\alpha = 29^\circ$ .

\* denotes cell aspect ratio  $\approx 1.62$ .

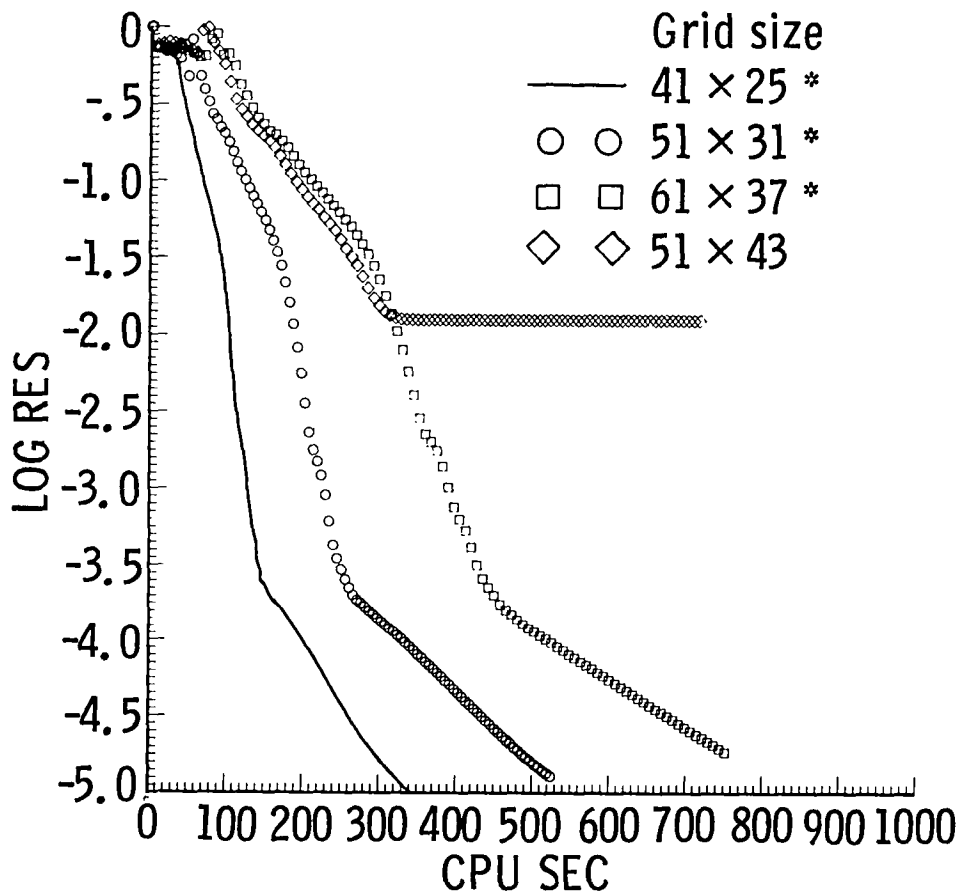


Figure 6. Convergence histories for different grid sizes for 2-D shock-reflection.  $M_\infty = 2.9$ ,  $\alpha = 23^\circ$ .

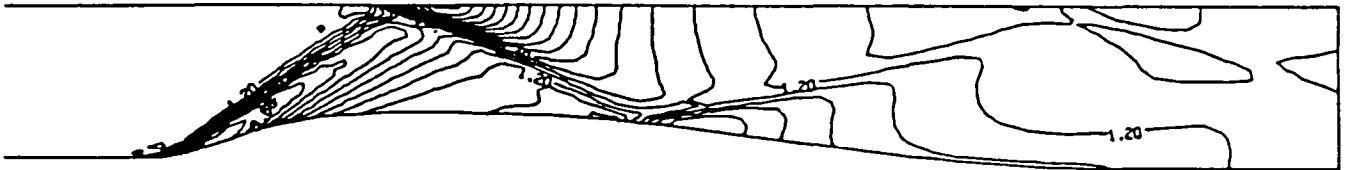


Figure 7. Contour plot of computed pressure for 2-D nozzle.  $M_{in} = 3.5$ .

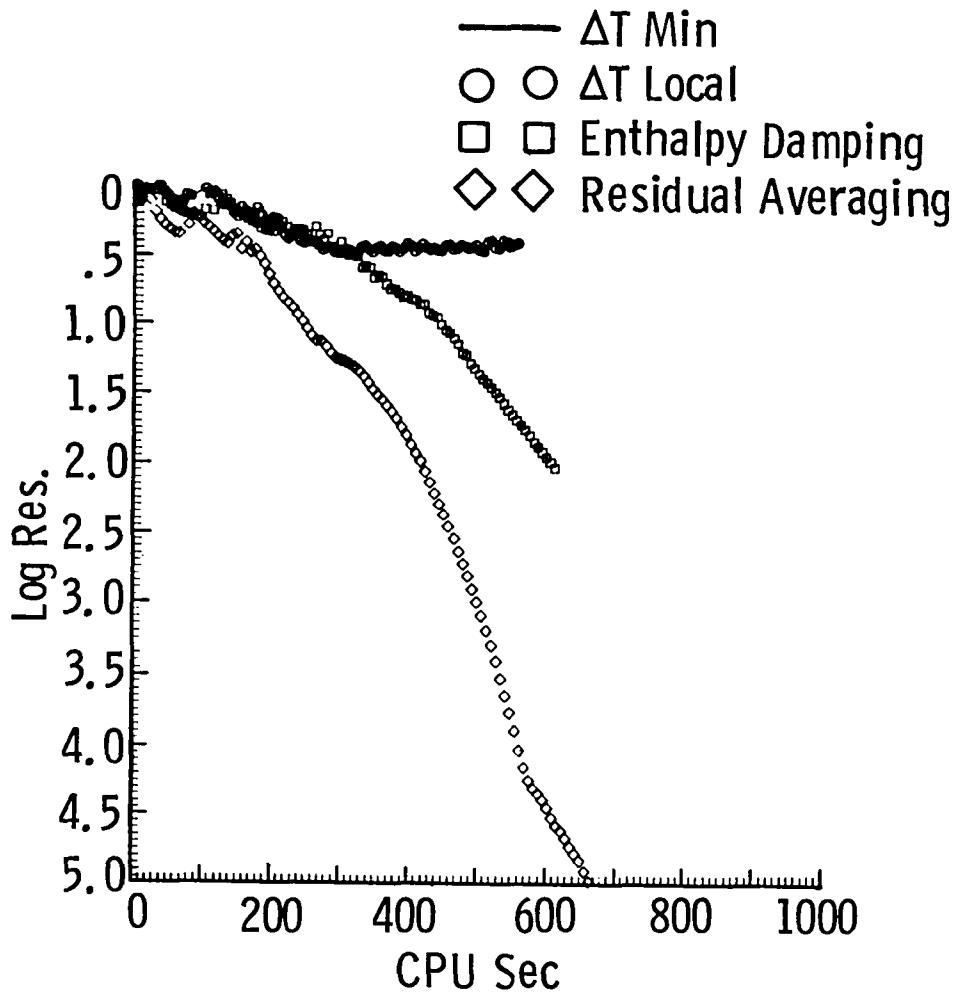


Figure 8. Convergence histories for different accelerating techniques for 2-D nozzle.  $M_{in} = 3.5$ .

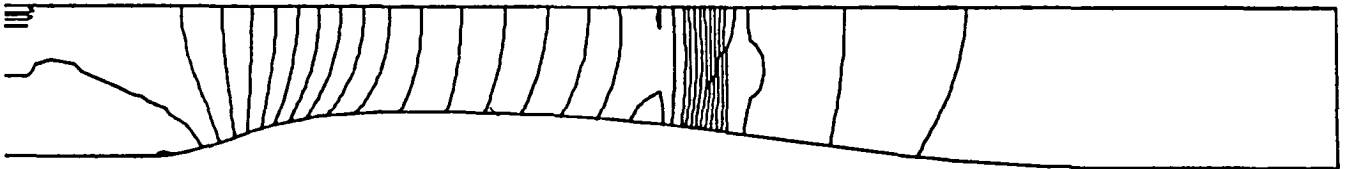


Figure 9. Contour plot of computed pressure for 2-D nozzle.  $M_{in} \approx 0.46$ .

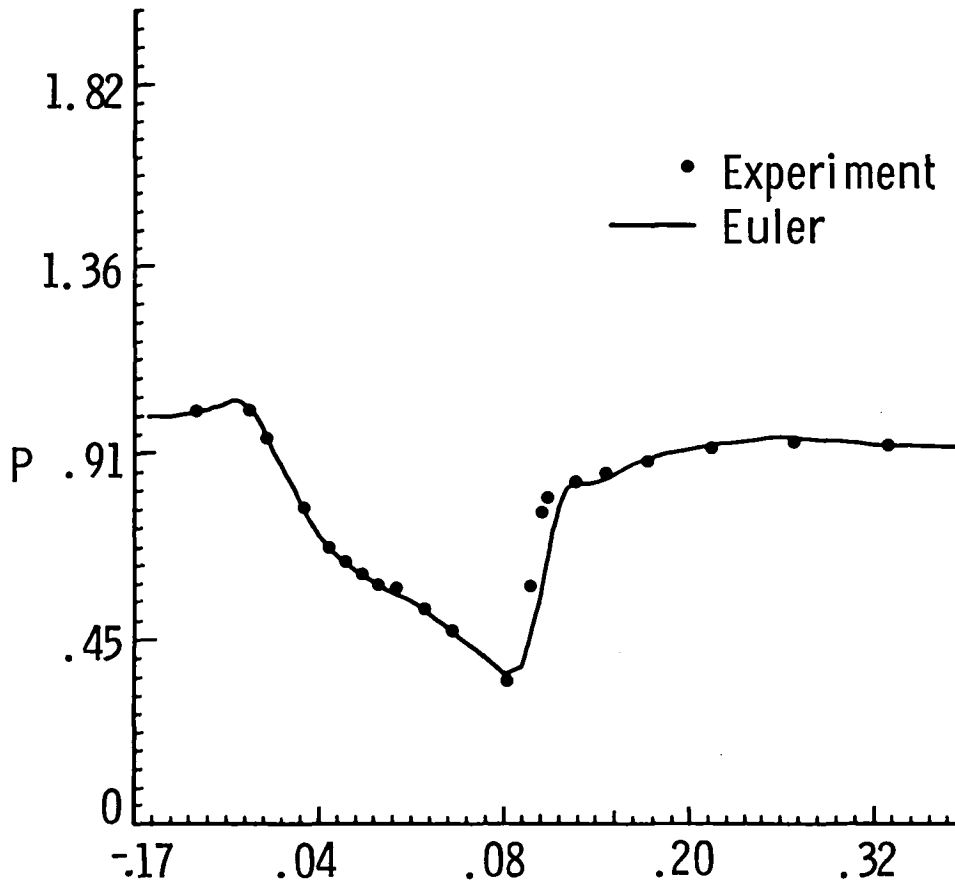


Figure 10. Comparison of computed and experimental surface pressure for 2-D nozzle.  $M_{in} \approx 0.46$ .



1. Report No. NASA CR-178053 ICASE Report No. 86-5		2. Government Accession No.		3. Recipient's Catalog No.	
4. Title and Subtitle  APPLICATION OF A RUNGE-KUTTA SCHEME FOR HIGH-SPEED INVISCID INTERNAL FLOWS				5. Report Date January 1986	
				6. Performing Organization Code	
7. Author(s)  Anutosh Moitra, Eli Turkel, and Ajay Kumar				8. Performing Organization Report No. 86-5	
				10. Work Unit No.	
9. Performing Organization Name and Address Institute for Computer Applications in Science and Engineering Mail Stop 132C, NASA Langley Research Center Hampton, VA 23665-5225				11. Contract or Grant No. NAS1-17070; NAS1-18107	
				13. Type of Report and Period Covered Contractor Report	
12. Sponsoring Agency Name and Address  National Aeronautics and Space Administration Washington, D.C. 20546				14. Sponsoring Agency Code 505-31-83-01	
				15. Supplementary Notes  Langley Technical Monitor: J. C. South  Final Report	
16. Abstract  A multi-stage Runge-Kutta method is analyzed for solving the two-dimensional Euler equations for external and internal flow problems. Subsonic, supersonic and, highly supersonic flows are studied. Various techniques for accelerating the convergence to a steady state are described and analyzed. Effects of the grid aspect ratio on the rate of convergence are evaluated. An enthalpy damping technique applicable to supersonic flows is described in detail. Numerical results for supersonic flows containing both oblique and normal shocks are presented confirming the efficiency of the method.					
17. Key Words (Suggested by Authors(s))  Euler, Runge-Kutta, high-speed, internal flow				18. Distribution Statement  34 - Fluid Mechanics & Heat Transfer  Unclassified - unlimited	
19. Security Classif.(of this report) Unclassified		20. Security Classif.(of this page) Unclassified		21. No. of Pages 26	22. Price A03



